

Increased Association of ZO-1 With Connexin43 During Remodeling of Cardiac Gap Junctions

Ralph J. Barker, Robert L. Price, Robert G. Gourdie

Abstract—The intercellular geometry of connexin43 (Cx43) gap junctional coupling is key to coordinated spread of electrical activation through the ventricle of the mammalian heart. A progressive redistribution of electrical and mechanical junctions into intercalated discs occurs during postnatal development. Breakdown of disc-localized pattern in the adult heart, to recapitulate immature distributions, is thought to be key to the genesis of conduction disturbance and arrhythmia. Recently, ZO-1 (a PDZ-MAGUK protein), has been suggested to have a role in generating coupling geometries between myocytes. We therefore investigated the codistribution of ZO-1 with Cx43 and N-cadherin in the adult rat ventricle using quantitative immunoconfocal and immunoelectron microscopy. These analyses indicated that, whereas ZO-1 and Cx43 codistribute within discs, only low to moderate point-by-point colocalization of Cx43 and ZO-1 is found within these domains compared with the relatively high level of colocalization between N-cadherin and ZO-1. By contrast, levels of association between Cx43 and ZO-1 increased rapidly and significantly ($P < 0.001$) after partial or complete enzymatic dissociation of myocytes from intact ventricle—a treatment known to induce gap junction endocytosis. Coimmunoprecipitation using Cx43- and ZO-1-specific antibodies confirmed that significantly ($P < 0.03$) increased ZO-1 is precipitated relative to Cx43 in freshly dissociated myocytes as compared with intact ventricle. On immunoblots, decreases in Cx43 relative mobility, consistent with increased phosphorylation, were observed following myocyte dissociation. The increased ZO-1-Cx43 association that occurs after remodeling of myocyte intercellular contacts indicates the possibility of unanticipated roles for ZO-1 in gap junction turnover during cardiac development and disease processes. (*Circ Res.* 2002;90:317-324.)

Key Words: heart ■ gap junction ■ connexin ■ PDZ ■ ZO-1

The gap junction (GJ) is an aggregate of channels that functions in intercellular communication by directly linking the cytoplasm of adjacent cells.¹ These channels provide a pathway for metabolic coupling and homeostatic exchange of molecules, as well as for propagation of electrical activation in excitable tissues such as the heart.²⁻⁵ Each of the apposed membranes in a GJ is composed of a honeycomb-like array of transmembrane channels termed connexons. Connexons from adjacent cells combine to form an intercellular channel that permits particles of less than 1000 Daltons to pass freely. Connexons, in turn, are composed of 6 protein subunits known as connexins, of which multiple subtypes exist in various animal species, cells, and tissue types. In the atrial and ventricular myocardia of adult and developing mammalian heart, connexin43 (Cx43)-containing GJs contribute to low-resistance pathways for propagation of electrical activation.¹⁻⁷ Atrial myocardium furthermore expresses Cx40 and Cx45, connexins also found in the pacemaker and conduction systems.^{3-5,7}

In the mammalian neonate, GJs and Ca^{2+} -dependent adhesion junctions (adherens junctions and desmosomes) are

distributed uniformly across the sarcolemma of ventricular myocytes.⁸⁻¹⁰ During postnatal development, the distribution of these junctions undergo a progressive remodeling, leading to the development of a highly organized structure at myocyte termini known as the intercalated disc. There is a lag in the rate at which GJs accrue at the disc compared with that of mechanical junctions.¹⁰ The eventual preferential colocalization of GJs at intercalated discs is a significant component of the normal maturation of electromechanical function and stability of cardiac activation.^{11,12} The understanding of the mechanisms regulating differentiation of cell-cell contacts at intercalated discs has pertinence to human cardiac disease.^{2,4,13} Breakdown of disc localization of GJs in ventricular myocardium¹³ and, as recently reported by Chien and co-workers in conduction tissues,¹⁴ to recapitulate distributions found at immature developmental stages may be a key factor in the genesis of conduction disturbance and arrhythmia.

The mechanisms involved in cumulative targeting of Cx43-GJs to the intercalated disc are uncharacterized. At present, 2 hypotheses have been proposed to explain how GJs

Original received July 3, 2001; resubmission received October 24, 2001; revised resubmission received December 10, 2001; accepted December 19, 2001.

From the Departments of Cell Biology and Anatomy (R.J.B., R.G.G.), Medical University of South Carolina, Charleston, SC; and the Department of Developmental Biology and Anatomy (R.L.P.), University of South Carolina School of Medicine, Columbia, SC.

Correspondence to Dr Robert G. Gourdie, Depts of Cell Biology and Anatomy, MUSC, 173 Ashley Ave, Suite 601, Charleston, SC 29425. E-mail gourdier@musc.edu

© 2002 American Heart Association, Inc.

Circulation Research is available at <http://www.circresaha.org>

DOI: 10.1161/hh0302.104471

become preferentially localized to this region of specialized sarcolemma. In the first, it has been independently suggested by 2 groups that there may be different rates of turnover of GJs in different domains of sarcolemma.^{10,15} In particular, it has been proposed that GJs associated with concentrations of adhesion junctions at the disc are preferentially maintained over GJs located in myocyte lateral domains. In the second hypothesis, Cx43-containing GJs are actively maintained at the intercalated disc via direct interactions with cytoskeletal-related anchoring or adapter proteins and other disc components. This latter hypothesis has received support from identification of zonula occludens-1 (ZO-1), a PDZ domain-containing protein localized at the intercalated disc,^{16–18} as a candidate molecule mediating anchorage of Cx43 to the cytoskeleton. Originally discovered in association with the tight junction plaque, ZO-1 is one member of the membrane-associated guanylate kinase family, which are known to function in protein targeting, signal transduction, and determination of cell polarity.¹⁹ ZO-1 has been linked to the function of tight junctions,¹⁹ adherens junctions,¹⁶ and more recently, GJs.^{17,18,20} Evidence supporting protein-protein interactions between Cx43 and ZO-1 have come from landmark work involving coimmunoprecipitation^{17,18} and the yeast 2-hybrid system.²⁰ Together this work has shown that the terminal 5 amino acids (DDLEI) of Cx43 bind the second PDZ domain of ZO-1 and that this interaction may be regulated by src-tyrosine phosphorylation of Cx43.¹⁸

In the following study, we have used immunoconfocal, immunoelectron microscopy, and coimmunoprecipitation to examine the relationship between Cx43 and ZO-1 in the ventricular myocardium of the adult rat heart. Our data indicate that association between ZO-1 and Cx43 is surprisingly limited to low to moderate levels in intact ventricular myocardium. Furthermore, we find that disruption of intercellular contacts between myocytes, a treatment inducing gap junction endocytosis,²¹ results in a dynamic change in the pattern of association between ZO-1 and Cx43. Our data suggests previously unanticipated roles for ZO-1 in the turnover of Cx43 during, or after, gap junctional endocytosis.

Materials and Methods

Myocyte Isolation

All reagents were purchased from Sigma Chemical Company, unless otherwise indicated. In this and subsequent procedures, 90-day-old (adult) Holtzman Sprague-Dawley rats were used. Rats were purchased from Harlan Biosciences (Indianapolis, Ind). Experiments were conducted in accordance with the Guide for the Use of Experimental Animals at the Medical University of South Carolina and conformed to the *Guide for the Care and Use of Laboratory Animals* published by the NIH (Publication No. 85-23, revised 1985). The myocyte isolation procedure used was based on the Langendorff perfusion method developed by Isenberg and Klockner²² with minor modifications (see expanded Materials and Methods section in the online data supplement available at <http://www.circresaha.org>).

Immunoconfocal and Immunoelectron Microscopy

Immunolabelings of ZO-1 (rabbit polyclonal, Zymed Laboratories, San Francisco, Calif), Cx43 (mouse monoclonal, Chemicon International, Temecula, Calif), and N-cadherin (mouse monoclonal) were carried out and imaged on a BioRad MRC 1024 laser scanning confocal microscope (LSCM) using standard protocols outlined

previously^{10,23} (see data supplement). Double immunolabelings were done using FITC and CY-5 secondary fluors to eliminate “bleed over” between detection channels. For immunoelectron microscopy, ventricular samples were prepared as previously described,²⁴ with modifications as outlined (see data supplement), labeled using a rabbit polyclonal antibody directed against ZO-1 (Zymed), and viewed on a JEOL 200CX EM.

Western Blotting

Immunoblotting was carried out using standard methodologies as outlined previously²³ with slight modifications (see data supplement). Primary antibodies used were against Cx43 (Sigma rabbit polyclonal anti-Cx43) and ZO-1 (Zymed rabbit anti-ZO-1). NIH Image was used for densitometric analyses of gels scanned on a ChemImager gel imager (Alpha Innotech Corp).

Immunoprecipitation-Immunoblotting

The immunoprecipitation method used was based on a protocol by Lukas et al²⁵ with modifications (see data supplement). Immunoprecipitations were performed using 2 anti-Cx43 antibodies against independent Cx43 epitopes (Sigma rabbit polyclonal anti-Cx43 No. C6219, Zymed polyclonal rabbit anti-Cx43 No. 71-0700). To confirm reproducibility, immunoprecipitations were repeated at least 3 times. To test specificity of the reaction, further control immunoprecipitations were carried out in the presence of a peptide inhibitor (Zymed polyclonal rabbit anti-Cx43 peptide). Immunoblots were performed to detect Cx43 and ZO-1 as described.

Colocalization and Statistical Analyses

FITC and CY-5 channels were thresholded to precisely match immunolabeling patterns as previously described,^{10,23} superimposed, and ZO-1 particles overlapping Cx43 particles were counted. The area of thresholded Cx43 particles and area of myocyte profile were also measured using NIH Image software. A pixel-by-pixel colocalization analysis, using proprietary BioRad software, was also used to assess levels of ZO-1 colocalization with Cx43. One-way ANOVAs were carried out on the data using Minitab statistical software. A more detailed description of the colocalization and statistical analyses is given in the expanded Materials and Methods section that can be found in the online data supplement available at <http://www.circresaha.org>.

Results

Cx43 and ZO-1 Show Limited

Coimmunolocalization Within Intercalated Discs

Consistent with previous findings, our immunoconfocal surveys of rat ventricle confirmed that ZO-1 was localized in endothelial tissues, interstitial cells, and at zones of cell-to-cell contact between myocytes, including intercalated discs.^{17,18,26} To examine association between ZO-1 and Cx43 or N-cadherin at intercalated discs in detail, we next performed double immunolabelings followed by optical sectioning at high resolution on the confocal microscope.

Initially, analyses were confined to sections of ventricular myocytes arrayed longitudinally (Figure 1). In such perspectives, discs are typically resolved as linear profiles. These studies confirmed that Cx43, N-cadherin, and ZO-1 were all localized within intercalated discs. However, detailed inspection and analysis of immunofluorescence colocalization indicated that the proportional degree of point-by-point overlap between Cx43 and ZO-1 immunolabeling was not as high as that of N-cadherin and ZO-1 (compare Figures 1a and 1b with 1c and 1d).

The difference in relative levels of colocalization was more apparent if discs were optically sectioned and reconstructed

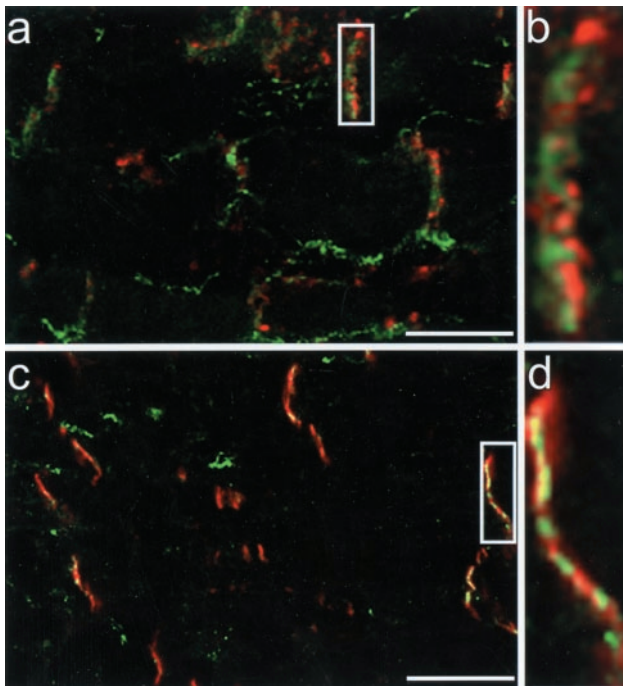


Figure 1. a and b, Cx43 (red-CY-5 secondary fluor) and ZO-1 (green-FITC secondary fluor); c and d, N-cadherin (red-CY-5) and ZO-1 (green-FITC) double immunolabelings in intact ventricular myocardium. Overlap between the fluors is shown in yellow. Details shown in b and d correspond to the boxed regions in a and c. Scale bar=25 μ m.

en face (Figure 2 and 3). In such views, components of the disc may be observed as part of an extended 2-dimensional surface.²⁷ Although points of overlap occurred between immunolabeled ZO-1 and Cx43, for the most part, the 2 immunolocalized proteins appeared to have relatively independent patterns of distribution (Figures 2a through 2c). A view of the signal channel images for Cx43 (Figures 2d through 2f) and ZO-1 (Figures 2g through 2i) in the same single optical sections confirms that the signal overlap between these 2 proteins is low to moderate. In contrast, ZO-1 and N-cadherin colocalized at relatively much higher spatial

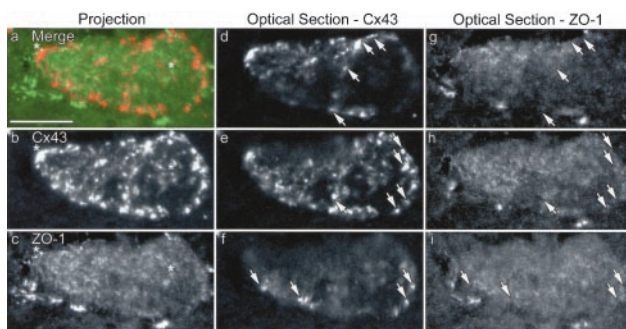


Figure 2. a through c, 3-D reconstruction of a ventricular intercalated disc in en face orientation immunolabeled for Cx43 in red and ZO-1 in green (a), with single channel perspectives of Cx43 and ZO-1 in b and c, respectively. *Cx43 and ZO-1 colocalizations. d through f and g through i, Single optical sections of Cx43 and ZO-1 labelings, respectively, through the disc. Arrows point to Cx43 immunopositive structures that show low levels of colocalization with ZO-1. Scale bar=5 μ m.

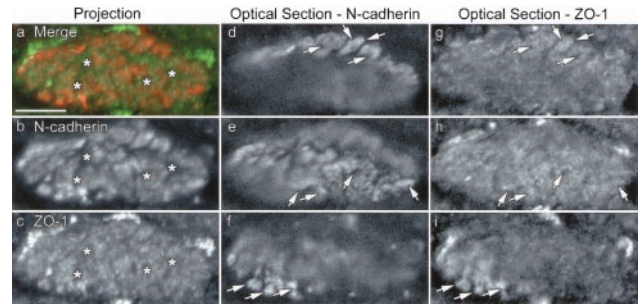


Figure 3. a through c, 3-D reconstruction of an intercalated disc immunolabeled for N-cadherin in red and ZO-1 in green (a), with single channel perspectives shown of N-cadherin and ZO-1 in b and c, respectively. *Areas in which both N-cadherin and ZO-1 signal are correspondingly low. d through f and g through i, Single optical sections of N-cadherin and ZO-1 labelings, respectively, through the disc. Arrows indicate areas of significant colocalization. Scale bar=5 μ m.

densities in these en face disc perspectives (Figures 3a through 3c). A much higher degree of correspondence between the distribution of these proteins is apparent in the single optical sections labeled for N-cadherin (Figures 3d through 3f) and ZO-1 (Figures 3g through 3i).

Because the results outlined appeared to differ from previous reports, we examined the association between GJs and ZO-1 in intact adult ventricular myocardium using immunogold electron microscopy (EM). Ultrastructurally defined GJs and cell adhesion junctions were readily identified in ultrathin sections of adult ventricle labeled with antibodies against ZO-1. The undulating profiles of adherens junctions were always extensively labeled with gold particles (Figure 4a), including those directly adjacent GJs (Figure 4b). Similarly, vascular endothelial cells also showed prominent accumulations of gold particles at presumed tight junctions (data not

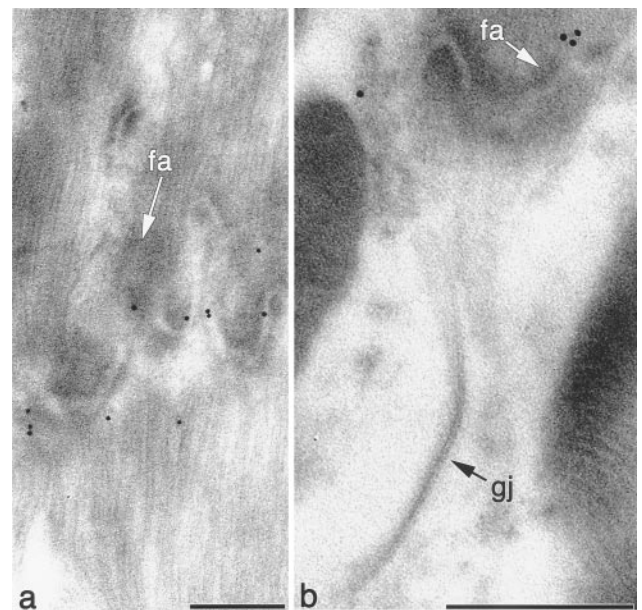


Figure 4. a and b, Immunogold electron microscopy of fascia adherens (labeled fa with white arrows in a and b) and gap junctions (labeled gj with black arrow in b) in ventricular myocardium. Scale bar=500 nm.

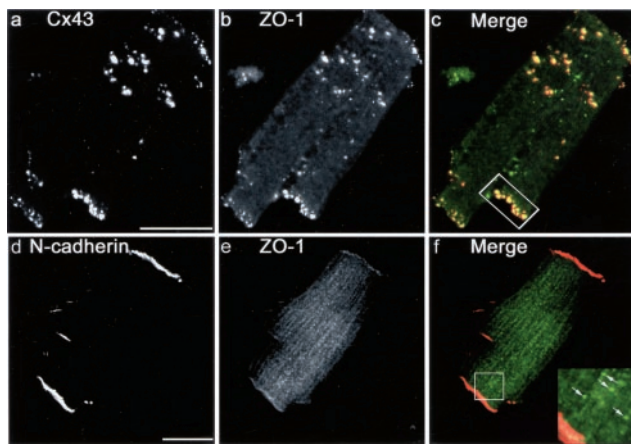


Figure 5. a through f, Freshly isolated ventricular myocytes immunolabeled for ZO-1 (FITC-green) and Cx43 or N-cadherin (CY-5-red). a and b show ZO-1 and Cx43 immunolabeling, respectively. c, Color merge of a and b. d and e, N-cadherin and ZO-1 immunolabeling, respectively. f, Color merge of d and e. The inset is of the boxed region in f. Internalized ZO-1 particles are indicated with arrows. Scale bars=50 μm .

shown). By contrast, though wholly consistent with the immunoconfocal analyses, all 22 ultrastructurally defined GJs observed in this survey showed no specific immunogold labeling (Figure 4b).

Colocalization of Cx43 and ZO-1 Increases After Dissociation of Ventricular Myocytes

Based on our immunoconfocal and immuno-EM data, we concluded that there was evidence for only limited colocalization between ZO-1 and Cx43 at intercalated discs in vivo. Nonetheless, the data for interaction between ZO-1 and Cx43 from the earlier coimmunoprecipitation and yeast hybrid studies were compelling.^{17,18,20} We speculated that if significant interaction occurred, it may be transient, and thus not easily resolved in intact myocardium. One well-characterized dynamic change in GJ distribution occurs following disruption of intercellular contacts. During isolation of adult cardiomyocytes, the entire population of GJs is internalized, undergoing redistribution from the sarcolemma to cytoplasmic vesicles known as annular GJs and cell surface located gap junctional vesicles.²¹ We therefore undertook immunoconfocal analyses of freshly isolated ventricular myocytes. In such cells, striking increases in levels of colocalization between immunolabeled Cx43 and ZO-1 were found (Figures 5a through 5c) relative to those observed at GJs in intact myocardium (Figures 1a and b). It should be noted that although association increased, a proportion of ZO-1-immunolabeled particles was not associated with Cx43 and vice versa. This increase in ZO-1-Cx43 colocalization is rapid, being detectable within 5 minutes of initiation of collagenase dissociation (Online Figure 1 available at <http://www.circresaha.org>). Interestingly, this figure also reveals immunolocalization of ZO-1 in myocyte nuclei in partially dissociated cells.

An increase in association after cell isolation was not observed between ZO-1 and N-cadherin (Figures 5d through 5f). Indeed, in freshly isolated ventricular myocytes, ZO-1 and N-cadherin colocalization appeared to decrease. Furthermore,

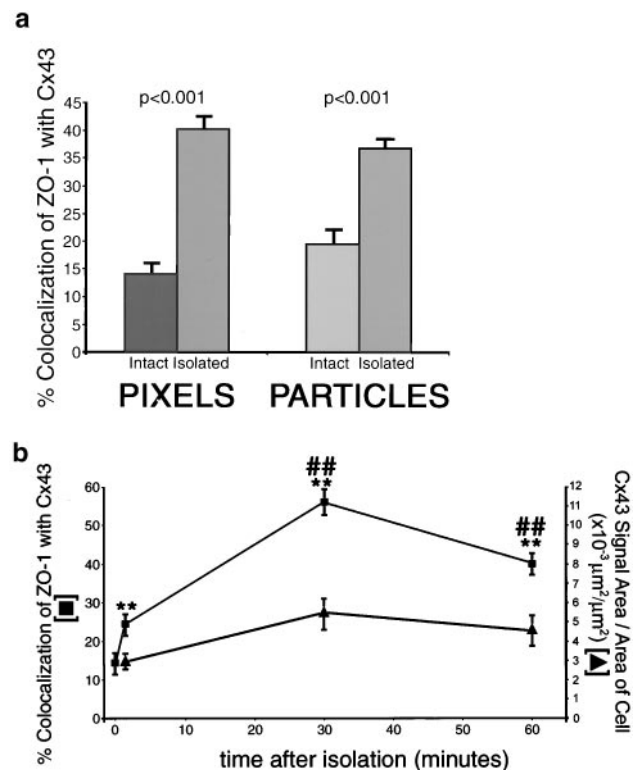


Figure 6. a, Cx43-ZO-1 colocalization analyses carried out pixel-by-pixel (PIXELS), or by Cx43 particle (PARTICLES), on optical sections of intact ventricular myocardium (intact) and isolated ventricular myocytes (isolated). Increases in ZO-1 colocalization with Cx43 measured within 60 minutes of dissociation, as determined by either quantitative method, were significant ($P<0.001$). b. On the left axis (squares), colocalization levels of ZO-1 with Cx43 (as determined by the pixel-by-pixel method on confocal optical sections) in intact ventricular myocardium (ie, the 0 time point) and isolated ventricular myocytes cultured for 1, 30, or 60 minutes after dissociation are plotted. **Difference between a given time point and the intact ventricular myocardial preparation that is significant at $P<0.01$. ##Difference between the 30- and 60-minute time points is significant at $P<0.01$ from the preceding time points. On the right x-axis (triangles), a corresponding time course is illustrated of Cx43 signal area (μm^2) per cell area after myocyte isolation.

whereas N-cadherin was maintained exclusively at the remnants of discs, clear dispersion of particulate ZO-1 to the cytoplasm was observed in isolated cells (Figure 5f, arrows inset). Presumably, a fraction of such ZO-1 particles were associated with internalized GJs, such as those seen in Figure 5c.

Next, we undertook quantitation of the colocalization between Cx43 and ZO-1 in the intact and dissociated ventricular preparations (Figure 6). This analysis was done using 2 approaches. In the first approach, we analyzed codistribution of Cx43 particles with ZO-1 in single optical sections of cells or tissues. Our presumption was that such particles corresponded to individual sarcolemma-localized or internalized (annular) GJs. Figure 6a (particles) shows that the degree of colocalization between Cx43 particles and ZO-1 particles increases significantly ($P<0.001$) following myocyte isolation. In the second approach (pixels, Figure 6a), we examined the pattern of colocalization on a pixel-by-pixel basis. The level of pixel-by-pixel colocalization increased over 3-fold

($P < 0.001$) following dispersion—a similar increase to that observed in the particle colocalization analysis. Finally, we undertook a 0- to 60-minute time course examining colocalization between Cx43 and ZO-1 following isolation of myocytes (Figure 6b). Colocalization percentages of ZO-1 with Cx43 approximately doubled in the first minute after myocyte isolation and climbed to a peak of 60% at 30 minutes before falling back to 40% after an hour of culture of isolated myocytes. Each change in colocalization percentage over this time course was significantly different ($P < 0.01$) from the time point preceding it. In contrast to the changing pattern of ZO-1-Cx43 association observed following myocyte dissociation, there was no significant variation in the area of Cx43 per cell over the time course examined (Figure 6b).

Coimmunoprecipitation Indicates an Increased Cx43 and ZO-1 Interaction and Potential Increases in Cx43 Phosphorylation After Myocyte Dissociation

Using anti-Cx43 antibodies, it was found that both Cx43 and ZO-1 could be coimmunoprecipitated, under nondenaturing conditions, from intact myocardium and freshly isolated myocytes (Figure 7a). Immunoprecipitations were performed using 2 anti-Cx43 antibodies against independent Cx43 epitopes. Western blots of ZO-1 and Cx43 immunoprecipitated by either of the anti-Cx43 antibodies used revealed that relatively more ZO-1 was consistently coimmunoprecipitated from isolated myocytes than intact myocardium. Densitometric analyses indicated that the relative level of ZO-1 (as a ratio of Cx43 levels in the sample) brought down by anti-Cx43 antibodies increased significantly ($P < 0.03$) between intact and isolated preparations (Figure 7b). Addition of peptide to which anti-Cx43 antibody was raised abolished immunoprecipitation of both Cx43 and ZO-1, indicating that the immunoprecipitation of ZO-1 was due to the specific interaction between Cx43 in the nondenatured preparations and the anti-Cx43 antibody (Figure 7a). Taken together, these data are consistent with the confocal colocalization analyses and strongly support that a rise in direct interaction between Cx43 and ZO-1 occurs after disruption of intercellular contact between myocytes.

The induction of endocytosis of Cx43-containing GJs in cultured cells has been reported to be associated with an increase in the phosphorylated isoforms of Cx43.²⁸ We therefore undertook Western blotting with emphasis on increasing separation in the 40- to 50-kDa range of protein relative mobility. These blots revealed that after dispersion of cardiac myocytes, there was a shift toward increased levels of higher molecular mass isoforms of Cx43 at 10, 30, and 60 minutes, as compared with Cx43 isoforms in intact myocardium (Figure 7c). The change in relative mobility of Cx43 has been correlated with changes in phosphorylation status of the protein. Thus, the decrease in relative mobility of Cx43 in PAGE following myocyte isolation likely corresponds to an increase in phosphorylated Cx43 isoforms. The majority of Cx43 protein detectable after myocyte isolation is consistent with a more phosphorylated form of Cx43. A comparison between the lanes of the Western blot shown in Figure 7c indicates that there is no decrease in Cx43 protein in the

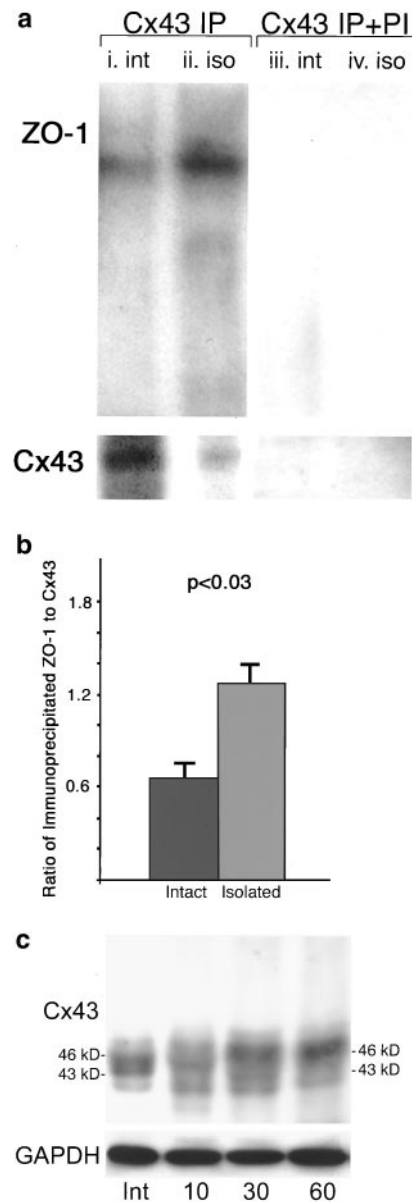


Figure 7. a, Western blots of Cx43 and ZO-1 in anti-Cx43 immunoprecipitates from intact myocardium (i. int) and isolated myocytes (ii. iso). Preincubation with peptide to which the Cx43 antibody was raised (Cx43 IP+PI) inhibited immunoprecipitation of Cx43 and ZO-1 from both intact (iii. int) and isolated (iv. iso) samples. b, Ratios of immunoprecipitated Cx43 to ZO-1 in intact or isolated cells. The difference between ratios is significant at $P < 0.03$. c, Anti-Cx43 and anti-GAPDH Western blots of intact myocardium (int) and myocytes isolated for 10, 30, and 60 minutes.

post-isolation time course relative to immunoblotted GAPDH levels.

Discussion

Here, using high-resolution analyses, we show that ZO-1 and Cx43 have low to moderate point-by-point colocalization within intercalated discs in normal ventricular myocardium. This is in contrast to the precise and extended pattern of colocalization observed between ZO-1 and N-cadherin, a component of fascia adherens. Relative levels of association

between Cx43 and ZO-1 increase conspicuously after dissociation of living ventricular myocytes from intact heart. Previous workers have characterized that this treatment, which results in the break-up of electrical and mechanical intercellular couplings, induces the formation of cytoplasmic gap junctional vesicles known as annular junctions.²¹ That this increase in ZO-1 immunolocalization at internalized GJs is accompanied by increases in direct interaction between Cx43 and ZO-1 at the protein-protein level is supported by coimmunoprecipitation analyses. Taken together, our findings are consistent with the growing evidence^{29,30} that previously hypothesized functions for MAGUK proteins (eg, ZO-1, dlg, PSD-95 and PSD-93) in active localization of proteins to membrane subdomains and in ion channel aggregation may need reevaluation, or at least, expansion to consider other possible modalities. Indeed, although an involvement of ZO-1 in stabilization and function of GJ channel clusters at intercalated discs remains possible, our data are also consistent with ZO-1 partnering with Cx43 subsequent to the disruption of functional communicative contact between myocytes. A similar conclusion has recently been reported in 42GPA9 Sertoli cells treated with lindane.³¹

Previous reports have suggested that ZO-1 may be an important factor in the intercalated disc-targeting and function of Cx43-containing cardiac GJs.^{17,18,20} These conclusions were based largely on studies of cultured cells, and included coimmunoprecipitation, yeast 2-hybrid assays, transfection experiments, and low-resolution single immunolabelings of Cx43 and ZO-1. To date, high-resolution immunoconfocal or immuno-EM analyses of the pattern of association within intact myocardial preparations have not been undertaken. Together, with data from coimmunoprecipitation experiments, our detailed spatial analyses indicate that low to moderate levels of Cx43-ZO-1 association occurs in normal adult myocardium. The results shown here nonetheless are consistent with those of previous reports in that significant contact between these 2 proteins can occur in cells *in vivo*, albeit under specific circumstances; namely, ZO-1-Cx43 interactions appear to be particularly increased at former GJs, internalized within living ventricular myocytes.

Previous studies of isolated myocytes suggest that all gap junctional membrane is immediately internalized (ie, no gap junctional membrane remains exposed to the myocyte exterior) directly following myocyte dissociation.²¹ The majority (>70% in rabbit and guinea pig) of these junctions in freshly dissociated cells are annular gap junctions. This internalization occurs mainly at or just subjacent to sites at which former cell contact occurred, including near the remnants of intercalated discs.²¹ Over time courses, annular gap junctions did not undergo significant reduction in number (ie, did not break down) nor did they traffic more deeply into the myocyte interior from initial subsarcolemmal locations. There was no apparent evidence for repopulation of gap junctions to the cell surface. As such, all Cx43 immunolabeling shown in Figure 5 is internalized and probably mostly located within annular gap junctions.

In guinea pig, though 77% of junctions in isolated myocytes at time zero are annular gap junctions, the percentage rises to 91.5% after a few hours.²¹ This has been interpreted

as evidence that in guinea pig, gap junction endocytosis continues following dissociation. The rat undergoes a similar progressive time course of gap junction endocytosis following dissociation of myocytes.³² It is thus possible that a progressive time course of gap junction endocytosis after cellular dissociation explains, or at correlates with, the cumulative time course of Cx43-ZO-1 colocalization that we show in Figure 6b.

Although a distinction should be drawn between processes occurring *in vivo* and those resulting from enforced cellular dissociation, annular GJs have been shown in a wide range of normal and diseased tissues. Intact myocardial tissues in which internalized GJ vesicles have been located include mammalian myocardium during early postnatal life³³ and adult hearts affected by myocardial pathologies.³⁴ Nonmyocardial tissues in which annular GJs have been observed include ovarian granulosa cells, bone, iris epithelium, oral epithelium, hepatocytes, and embryonal carcinoma cells.³⁵ More recently, Laird et al³⁶ used GFP-tagged Cx43 to provide direct evidence that annular GJ formation is a normal mechanism for removal and turnover of membrane channel aggregates. On an ultrastructural scale, this study reveals that the process is swift and dramatic. Within minutes, GJs are torn as extended bi-membranous structures from the plasma membrane and internalized intact within a neighboring cell. On the basis of these *in vivo* and *in vitro* studies, it is probable that rapid generation of cytoplasmic GJ vesicles is "part and parcel" of the remodeling of cell-cell contacts that occurs during normal developmental and disease processes. Finally, consistent with the low levels of ZO-1-Cx43 association we report in undisturbed ventricular muscle, it is noteworthy that annular GJs are rare in nondiseased myocardial tissues from adult mammals.^{33,34}

One reason that we initially focused on internalized GJs as a potential target for increased Cx43-ZO-1 interaction is that earlier workers had reported that elements of the actin cytoskeleton were closely associated with annular junctions.^{37,38} As the C-terminal of ZO-1 is thought to interact with the actin cytoskeleton,^{16,17} we reasoned that ZO-1 may also be localized to annular GJs. A logical extension then is to surmise that ZO-1 may be involved in the generation of these cytoplasmic membrane structures *per se*. Actin is known to directly participate in endocytosis processes,³⁹ including specific involvement in GJ endocytosis.³⁸ ZO-1, via its ability to simultaneously interact with Cx43 and cytoskeleton, may confer specificity to actin-based contractile processes. The tearing out and internalization of structures as large and potentially noncompliant as GJ channel clusters *in toto* presumably requires powerful, site-directed mechanisms of force generation.

A putative role for ZO-1 in GJ endocytosis re-raises the prospect for ZO-1 involvement in generation of myocyte coupling patterns in development and disease, although not necessarily just as a multivalent adapter, stabilizing the components of electrical and mechanical junctions within intercalated discs. We have formerly hypothesized that discs at myocyte termini may differentiate by mechanisms that include more rapid turnover of Cx43-containing GJs at lateral domains of ventricular myocytes.¹⁰ Interestingly, annular GJs

are significantly more common in ventricular muscle during the postnatal period in which intercalated disc differentiation occurs.³³ Whether this internalized GJ population in postnatal myocardium has associated ZO-1 remains to be explored. Other explanations of the increased association of Cx43 and ZO-1 after cell dissociation also deserve consideration. These alternates would include roles for ZO-1 in targeting of annular GJs to the lysosome and/or recycling of Cx43 from annular junctions back to functional GJs in the plasma membrane.

Phosphorylation of Cx43 represents an important mechanism for the regulation of GJ gating, assembly, trafficking, and degradation.^{40,41} Cx43 in normal intact myocardium can be resolved into 2 distinct phosphorylated species on Western blotting, although as many as 5 species have been reported.⁴² We found that an increase in potential Cx43 phosphoisoforms, as discriminated by electrophoretic mobility shift, consistently accompanies myocyte isolation and the induction of GJ endocytosis. A similar decrease of the relative mobility of Cx43 on immunoblots has been previously reported following induction of GJ endocytosis in studies of cultured cell lines.²⁸ Further evidence supporting our observation comes from reports that antibodies specific for the nonphosphorylated isoform of Cx43 immunolocalize at internalized annular GJs at only relatively low levels.⁴² In this respect, it is also important to note that no overall alteration in Cx43 levels occurs over the time course following myocyte dissociation, as assessed by both immunofluorescence quantitation and immunoblotting. The changes in Cx43-ZO-1 association and Cx43 relative mobility observed in this study are therefore unlikely to be the result of selective degradation of gap junctions not containing phosphorylated Cx43 and not associated with ZO-1.

In conclusion, this study establishes a number of observations and raises some equally important questions. Based on the results, it seems that direct interactions between ZO-1 and Cx43 are dynamic and capable of undergoing rapid change after disruption of functional contact between myocytes. This change occurs over a specific time frame in living cells, with levels of association quantifiably rising and falling within 60 minutes of myocyte dissociation. Finally, the increased Cx43-ZO-1 interaction we observe is correlated with an equally rapid change in the relative mobility (and possibly phosphorylation status) of Cx43. Whether phosphorylation of Cx43 is a prerequisite for increased ZO-1-Cx43 interaction remains to be determined. Of other remaining questions, perhaps the most important is whether ZO-1 directly participates in GJ endocytosis. Future experiments targeting Cx43-ZO-1 interaction using dominant negative approaches might enable discrimination of whether this interaction is necessary during or subsequent to the genesis of annular GJs. Resolution of this question may provide important new avenues for understanding the mechanistic basis of gap junctional remodeling in cardiac development and disease.

Acknowledgments

This work was supported by grants from the NHLBI (HL56728) and National Science Foundation (9734406). The excellent technical assistance of Jeff Davis and Jane Jourdan is acknowledged with

gratitude. We thank Dr Cheng Gang for his suggestions and discussion.

References

- Goodenough DA, Goliger JA, Paul DL. Connexins, connexons, and intercellular communication. *Annu Rev Biochem.* 1996;65:475–502.
- Spach MS. Discontinuous cardiac conduction: its origin in cellular connectivity with long-term adaptive changes that cause arrhythmias. In: Soonper PM, Joyner RW, Jalife J, eds. *Discontinuous Conduction in the Heart*. New York, NY: Futura Publishing Company, Inc; 1997:5–51.
- Gros DB, Jongsma HJ. Connexins in mammalian heart function. *Bioessays.* 1996;18:719–730.
- Severs NJ. The cardiac muscle cell. *Bioessays.* 2000;22:188–199.
- Lo CW. Role of gap junctions in cardiac conduction and development: insights from the connexin knockout mice. *Circ Res.* 2000;87:346–348.
- Beyer EC, Paul DL, Goodenough DA. Connexin43: a protein from rat heart homologous to a gap junction protein from liver. *J Cell Biol.* 1987;105:2621–2629.
- Thomas SA, Schuessler RB, Berul CI, Beardslee MA, Beyer EC, Mendelsohn ME, Safitz JE. Disparate effects of deficient expression of connexin43 on atrial and ventricular conduction: evidence for chamber-specific molecular determinants of conduction. *Circulation.* 1998;97:686–691.
- Gourdie RG, Green CR, Severs NJ, Thompson RP. Immunolabelling patterns of gap junction connexins in the developing and mature rat heart. *Anat Embryol (Berl).* 1992;185:363–378.
- Fromaget C, el Aoumari A, Gros D. Distribution pattern of connexin 43, a gap junctional protein, during the differentiation of mouse heart myocytes. *Differentiation.* 1992;51:9–20.
- Angst BD, Khan LU, Severs NJ, Whitely K, Rothery S, Thompson RP, Magee AI, Gourdie RG. Dissociated spatial patterning of gap junctions and cell adhesion junctions during postnatal differentiation of ventricular myocardium. *Circ Res.* 1997;80:88–94.
- Spach MS, Heidlage JF, Dolber PC, Barr RC. Electrophysiological effects of remodeling cardiac gap junctions and cell size: experimental and model studies of normal cardiac growth. *Circ Res.* 2000;86:302–311.
- Gutstein DE, Morley GE, Tamaddon H, Vaidya D, Schneider MD, Chen J, Chien KR, Stuhlmann H, Fishman GI. Conduction slowing and sudden arrhythmic death in mice with cardiac-restricted inactivation of connexin43. *Circ Res.* 2001;88:333–339.
- Severs NJ. Cardiovascular disease. *Novartis Found Symp.* 1999;219:188–206; 206–211.
- Nguyen-Tran VT, Kubalak SW, Minamisawa S, Fiset C, Minamisawa S, Fiset C, Wollert KC, Brown AB, Ruiz-Lozano P, Barrere-Lemaire S, Kondo R, Norman LW, Gourdie RG, Rahme MM, Feld GK, Clark RB, Giles WR, Chien KR. A novel genetic pathway for sudden cardiac death via defects in the transition between ventricular and conduction system cell lineages. *Cell.* 2000;102:671–682.
- Saffitz JE, Green KG, Kraft WJ, Schechtman KB, Yamada KA. Effects of diminished expression of connexin43 on gap junction number and size in ventricular myocardium. *Am J Physiol Heart Circ Physiol.* 2000;278:H1662–H1670.
- Itoh M, Nagafuchi A, Moroi S, Tsukita S. Involvement of ZO-1 in cadherin based cell adhesion through its direct binding to α catenin and actin filaments. *J Cell Biol.* 1997;138:181–192.
- Toyofuku T, Yabuki M, Otsu K, Kuzuya T, Hori M, Tada M. Direct Association of the gap junction protein connexin 43 with ZO-1 in cardiac myocytes. *J Biol Chem.* 1998;273:12725–31.
- Toyofuku T, Akamatsu Y, Zhang H, Kuzuya T, Tada M, Hori M. c-Src regulates the interaction between connexin-43 and ZO-1 in cardiac myocytes. *J Biol Chem.* 2001;19:276:1780–1788.
- Stevenson BR, Keon BH. The tight junction: morphology to molecules. *Annu Rev Cell Dev Biol.* 1998;14:89–109.
- Giepmans BNG, Moolenaar WH. The gap junction protein connexin43 interacts with the second PDZ domain of the zona occludens-1 protein. *Curr Biol.* 1998;8:931–934.
- Severs NJ, Shovel KS, Slade AM, Powell T, Twist VW, Green CR. Fate of gap junctions in isolated adult mammalian cardiomyocytes. *Circ Res.* 1989;65:22–42.
- Isenberg G, Klockner U. Calcium tolerant ventricular myocytes prepared by incubation in a “KB medium”. *Pflügers Arch.* 1982;395:6–18.
- Litchenberg WH, Norman LW, Holwell AK, Martin KL, Hewett KW, Gourdie RG. The rate and anisotropy of impulse propagation in the

- postnatal terminal crest are correlated with remodeling of Cx43 gap junction pattern. *Cardiovasc Res*. 2000;45:379–387.
24. Price RL, Nakagawa M, Terracio L, Borg TK. Ultrastructural localization of laminin on in vivo embryonic, neonatal, and adult rat cardiac myocytes and in early rat embryos raised in whole-embryo culture. *J Histochem Cytochem*. 1992;40:1373–1381.
 25. Lukas J, Bartek J. Immunoprecipitation of proteins under nondenaturing conditions. In: Cellis JE, ed. *Cell Biology: A Laboratory Manual*. 2nd ed. Vol 4. New York, NY: Academic Press; 1998:489–494.
 26. Itoh M, Yonemura S, Nagafuchi A, Tsukita S, Tsukita S. A 220-kD undercoat-constitutive protein: its specific localization at cadherin-based cell-cell adhesion sites. *J Cell Biol*. 1991;115:1449–1462.
 27. Gourdie RG, Green CR, Severs NJ. Gap junction distribution in adult mammalian myocardium revealed by an anti-peptide antibody and laser scanning confocal microscopy. *J Cell Sci*. 1991;99:41–55.
 28. Guan X, Ruch RJ. Gap junction endocytosis and lysosomal degradation of connexin43-P2 in WB-F344 rat liver epithelial cells treated with DDT and lindane. *Carcinogenesis*. 1996;17:1791–1798.
 29. Migaud M, Charlesworth P, Dempster M, Webster LC, Watabe AM, Makhinson M, He Y, Ramsay MF, Morris RG, Morrison JH, O'Dell TJ, Grant SG. Enhanced long-term potentiation and impaired learning in mice with mutant postsynaptic density-95 protein. *Nature*. 1998;396:433–439.
 30. McGee AW, Topinka JR, Hahimoto K, Petralia RS, Kakizawa S, Kauer F, Aguilera-Moreno A, Wenthold RJ, Kano M, Brecht DS. PSD-93 knock-out mice reveal that neuronal MAGUKs are not required for development or function of parallel fiber synapses in cerebellum. *J Neurosci*. 2001;21:3085–3091.
 31. Defamie N, Mograbi B, Roger C, Cronier L, Malassine A, Brucker-Davis F, Feniche P, Segretain D, Pointis G. Disruption of gap junctional intercellular communication by lindane is associated with aberrant localization of connexin43 and zona occludens-1 in 42GPA9 Sertoli cell. *Carcinogenesis*. 2001;22:1537–1542.
 32. Mazet F, Wittenberg BA, Spray DC. Fate of intercellular junctions in isolated adult rat cardiac cells. *Circ Res*. 1985;56:195–204.
 33. Legato MJ. Cellular mechanisms of normal growth in the mammalian heart: II, a quantitative and qualitative comparison between the right and left ventricular myocytes in the dog from birth to five months of age. *Circ Res*. 1979;44:263–279.
 34. Uzzaman M, Honjo H, Takagishi Y, Emdad L, Magee AI, Severs NJ, Kodama I. Remodeling of gap junctional coupling in hypertrophied right ventricles of rats with monocrotaline-induced pulmonary hypertension. *Circ Res*. 2000;86:871–878.
 35. Larsen WJ. Biological implications of gap junction structure, distribution and composition. *Tissue Cell*. 1983;15:645–671.
 36. Laird DW, Jordan K, Shao Q. Expression and imaging of connexin-GFP chimeras in live mammalian cells. *Methods Mol Biol*. 2001;154:135–142.
 37. Larsen WJ, Tung HN, Murray SA, Swenson CA. Evidence for the participation of actin microfilaments and bristle coats in the internalization of gap junction membrane. *J Cell Biol*. 1979;83:576–587.
 38. Murray SA, Williams SY, Dillard CY, Narayanan SK, McCauley. Relationship of cytoskeletal filaments to annular gap junction expression in human adrenal cortical tumor cells in culture. *J Exp Cell Res*. 1997;234:398–404.
 39. Merrifield CJ, Moss SE, Ballestrem C, Imhof BA, Giese G, Wunderlich I, Almers W. Endocytic vesicles move at the tips of actin tails in cultured mast cells. *Nat Cell Biol*. 1999;1:72–74.
 40. Lampe PD, TenBroek EM, Burt JM, Kurata WE, Johnson RG, Lau AF. Phosphorylation of connexin43 on serine 368 by protein kinase C regulates gap junctional communication. *J Cell Biol*. 2000;149:1503–1512.
 41. Laird DW. The life cycle of a connexin: gap junction formation, removal, and degradation. *J Bioenerg Biomembr*. 1996;28:311–318.
 42. Nagy JJ, Li WE, Roy C, Doble BW, Gilchrist JS, Kardami E, Hertzberg EL. Selective monoclonal antibody recognition and cellular localization of an unphosphorylated form of connexin43. *Exp Cell Res*. 1997;236:127–136.

Circulation Research

JOURNAL OF THE AMERICAN HEART ASSOCIATION



Increased Association of ZO-1 With Connexin43 During Remodeling of Cardiac Gap Junctions

Ralph J. Barker, Robert L. Price and Robert G. Gourdie

Circ Res. 2002;90:317-324; originally published online January 3, 2002;

doi: 10.1161/hh0302.104471

Circulation Research is published by the American Heart Association, 7272 Greenville Avenue, Dallas, TX 75231

Copyright © 2002 American Heart Association, Inc. All rights reserved.

Print ISSN: 0009-7330. Online ISSN: 1524-4571

The online version of this article, along with updated information and services, is located on the World Wide Web at:

<http://circres.ahajournals.org/content/90/3/317>

Data Supplement (unedited) at:

<http://circres.ahajournals.org/content/suppl/2002/02/19/90.3.317.DC1>

Permissions: Requests for permissions to reproduce figures, tables, or portions of articles originally published in *Circulation Research* can be obtained via RightsLink, a service of the Copyright Clearance Center, not the Editorial Office. Once the online version of the published article for which permission is being requested is located, click Request Permissions in the middle column of the Web page under Services. Further information about this process is available in the [Permissions and Rights Question and Answer](#) document.

Reprints: Information about reprints can be found online at:

<http://www.lww.com/reprints>

Subscriptions: Information about subscribing to *Circulation Research* is online at:

<http://circres.ahajournals.org/subscriptions/>

DATA SUPPLEMENT

Materials and Methods.

Myocyte Isolation. All reagents were purchased from Sigma Chemical Company, unless otherwise indicated. The myocyte isolation procedure used was based upon a Langendorff perfusion method developed by Isenberg and Klockner¹. In this, and all subsequent procedures, 90 day old (adult) Holtzman Sprague-Dawley rats were used. Rats were anesthetized with ether, hearts were surgically removed and then perfused retrogradely through the aorta with warm (37°C) Joklik's S-MEM (Gibco) on a Langendorff apparatus. After five minutes, the perfusion solution was switched to Joklik's S-MEM with 30mM taurine, 1mM adenosine, 26 mM NaHCO₃, 25 mM glutamic acid, and 1 mg/mL of collagenase (Worthington Biochemical) for 10 minutes, then to KB solution (85 mM KCl, 30 mM K₂HPO₄, 5 mM MgSO₄, 5 mM Na₂ATP, 5 mM pyruvate, 5 mM succinate, 5 mM β-hydroxy-butyrate, 5 mM creatine, adjusted to pH 7.2 with KOH) for 5 minutes. Following collagenase perfusion, hearts were taken down, the ventricles extensively minced and then incubated at 37°C in KB media on an orbital shaker for variable periods of time. This solution was removed and run through steel mesh to separate cells, which were then pelleted by centrifugation at 1000rpm (10 minutes) on a Marathon 16K centrifuge (Fischer Scientific).

Immunoconfocal and Immunoelectron Microscopy. Immunoconfocal microscopy was performed according to protocols previously established with modifications as described below^{2,3}. For preparation of intact tissues, hearts from adult rats were surgically removed, or

taken down intact from the Langendorff perfusion apparatus following exposure to collagenase, and embedded in TBS tissue freezing compound (Triangle Biomedical Sciences, Durham, NC). The specimens were then immersed immediately in liquid nitrogen-cooled isopentane. Fresh frozen sections (10 μ m) were prepared at -32°C and placed on glass slides. Sections were fixed with 4% paraformaldehyde in phosphate buffered saline (PBS) for 10 minutes, washed 3x with PBS-A (PBS with 0.2% sodium azide) with 0.1% Triton X-100 added, and blocked with 1% bovine serum albumin (BSA) in PBS-A for 1 hour. Isolated adult rat ventricular myocytes were fixed in suspension with 4% paraformaldehyde for 10 minutes, then centrifuged for 10 minutes at 1000 rpm and washed 3x in PBS-A, then blocked with 1% BSA in PBS-A with 0.1% Triton X-100 added for 1 hour. Suspended cells were attached to glass slides for staining using Cel-Tak tissue adhesive (Becton-Dickinson).

Slides were incubated overnight at 4°C in a combination of primary antibodies directed against ZO-1 (rabbit polyclonal, Zymed Laboratories, San Francisco, CA), Cx43 (mouse monoclonal, Chemicon International, Temecula, CA), and N-cadherin (mouse monoclonal). Appropriate secondary antibodies (Molecular Probes) conjugated to fluorescein or CY-5 were used to label the primary antibodies. Double labelings were carried out using FITC and CY-5 secondary fluors, to eliminate any possibility of “bleed over” between detection channels. Slowfade Light anti-fade agent (Molecular Probes) was added and the sections were coverslipped and sealed. Slides were examined using a BioRad MRC 1024 laser scanning confocal microscope (LSCM).

For immuno-electron microscopy, intact ventricular myocardial tissue was dissected from adult rats and minced into chunks of less than 1mm. All materials for electron microscopy were obtained from Electron Microscopy Sciences (Ft. Washington, PA). Tissues were then fixed in

4% paraformaldehyde and 0.2% glutaraldehyde in Sorenson's phosphate buffer, pH 7.4, as previously described⁴. Samples were rinsed in PBS (pH 7.4), dehydrated through a graded ethanol series, embedded in Lowicryl K4M and polymerized by UV irradiation. Dehydration, embedding, and polymerization were carried out at -20°C. Sections (150-200nm) were stained using a rabbit polyclonal antibody directed against ZO-1 (Zymed) and a secondary goat anti-rabbit antibody conjugated to 10nm colloidal gold and viewed on a JEOL 200CX TEM at 160 and 200kV.

Western Blotting. Western blotting was performed according to protocols previously established with minor modifications as described below². Samples of ventricular myocardium from adult rats were snap frozen in liquid nitrogen. The tissues were then ground in a mortar and pestle which was kept cold in a liquid nitrogen bath. After grinding, samples were solubilized in sodium dodecyl sulfate (SDS) reducing buffer (60 mM Tris-HCl pH 6.8, 10% SDS, 20% glycerol) and sonicated at high power for 30 seconds. Samples were placed in an SDS-polyacrylamide gel electrophoresis (PAGE) using a Biorad Mini-Protean II Electrophoresis Cell. Following PAGE, gels were transferred to PVDF membranes (Biorad Laboratories) for one hour. Membranes were washed and blocked for one hour in TBS-T (100 mM Tris HCl pH 7.5, 770 mM NaCl) and 5% non-fat milk. Primary antibodies were added against Cx43 (Sigma rabbit polyclonal anti-Cx43) or ZO-1 (Zymed rabbit anti-ZO-1) for 1 hour. After washing 3x in TBS-T, secondary reagents linked to fluorescein (Molecular Probes) were added for one hour, then membranes were again washed 3x in TBS-T. Final detection was accomplished using an alkaline phosphatase conjugated anti-fluorescein antibody (Tropix Inc.) and ECL's CDP-Star system (Tropix Inc.). Results were recorded on chemiluminescent film (Amersham). The NIH

Image software (<http://rsb.info.nih.gov/nih-image>) was used for densitometric analyses of gels scanned on the ChemImager gel imager (Alpha Innotech Corp).

Immunoprecipitation. Immunoprecipitation was performed based on the protocol developed by Lukas et al.⁵. Samples of adult rat ventricular tissue (approximately 1mm x 1mm size) and freshly isolated adult rat ventricular myocytes were placed in ice-cold lysis buffer (1% Triton X-100, 0.5% NP-40, 20mM HEPES pH 7.4, 50mM sodium chloride, 1mM EGTA, 5mM β -glycerophosphate, 30mM sodium pyrophosphate, 1x Sigma protease inhibitor cocktail, 1x Sigma phosphatase inhibitor cocktail II) and homogenized by hand using a Elvjhem tissue grinder. Samples were incubated on ice for 30 minutes with vortexing and grinding every 5 minutes, then centrifuged at 8000rpm on a Marathon 16K centrifuge for 10 minutes. The supernatant was transferred to a fresh eppendorf tube. To preclear the solution of endogenous antibody, 40 μ l of protein A-agarose (Biorad) was added for 1 hour and the tubes were incubated at 4°C on a Nutator (Fischer). Tubes were spun for 30 sec at full speed to pellet protein A-agarose; the supernatant was then transferred to a new tube. 5mg of a anti-Cx43 primary antibody was added and the samples were incubated overnight at 4°C on a Nutator. 50mg of protein A-agarose was then added for 1 hour. The protein A-agarose-antibody was spun down 5x with washes in ice-cold lysis buffer after each spin. After the final spin, the supernatant was removed and 200ul of PSB was added. The solution was vortexed for 30 seconds and boiled at 95°C for 5 minutes. Immunoblot assays were then performed to detect Cx43 and ZO-1. Two anti-Cx43 antibodies raised against completely independent peptide epitopes from the C-terminal of Cx43 (Sigma rabbit polyclonal anti-Cx43 #C6219, Zymed polyclonal rabbit anti-Cx43 #71-0700) were used for the immunoprecipitations. To confirm reproducibility, immunoprecipitations were repeated at

least 3 times. To test specificity of the reaction, further control immunoprecipitations were carried out in the presence of a peptide inhibitor commercially available for one of the anti-Cx43 antibodies (Zymed polyclonal rabbit anti-Cx43 peptide).

Co-Localization and Statistical Analyses. 15-30 random optical sections double immunolabeled for Cx43 and ZO-1 from adult rat myocardium (from 3 rats) and freshly isolated adult rat ventricular cardiomyocytes (from 3 independent isolations) were taken on a BioRad MRC 1024 LSCM using a 40 x 1.4 NA Zeiss objective. Constant gain, black level and confocal iris settings were used for capture of each image. For particle analyses, information from FITC (ZO-1) and CY-5 (Cx43) channels were thresholded to precisely match immunolabeling patterns as previously described^{2,3,6}. NIH image was then used to count the number of Cx43 and ZO-1 particles in each channel (particles of 2 pixels in size or less were not counted). Next, thresholded particles in each channel were gray-level-encoded and superimposed. The frequency of Cx43 particles overlapping ZO-1 particles were then counted for each image. A pixel-by-pixel co-localization analysis, using proprietary BioRad software, was also used to assess levels of ZO-1 co-localization with Cx43. Data from confocal optical sections and scanned immunoblots were checked for normality and homogeneity of variance using Minitab. No transformations were required. One way ANOVA was carried out on the data using Minitab, a widely used statistical software program for the Power Mac which permitted basic statistical analyses. F statistics with p values above 0.05 were rejected as not significant. Data shown together with p values from ANOVAs include the mean and standard error of the mean.

Cx43 Quantitative Immunofluorescence Microscopy of Isolated Myocytes. Immunolabeled slides of isolated adult rat cardiomyocytes were prepared as described above. Sixteen random

single optical sections were taken of myocytes isolated on a Langendorff perfusion apparatus for 1, 30, and 60 minutes. Measurement of the area of gap junctions per cell area was performed as previously described¹ using NIH Image. Data was processed using Minitab computer software. One way ANOVA was performed. No significant difference in the amount of Cx43 per cell area was found between the three groups examined (1, 30, 60 minutes).

Data Supplement Figure 1. **a-c**, Immunolabeling for Cx43 (CY-5) and ZO-1 (FITC) in a partially collagenase-digested ventricular myocardial preparation. **a** and **b** are the single channel information for Cx43 and ZO-1 immunolabeling respectively. **c** is the color merge of these 2 channels (ZO-1-green, Cx43-red). Arrows indicate the partial separation of an intercalated disc. Asterisks indicate nuclear ZO-1 immunolabeling.

References.

1. Isenberg G, Klockner U. Calcium tolerant ventricular myocytes prepared by incubation in a “KB medium”. *Pflug Arch.* 1982;395:6-18.
2. Litchenberg WH, Norman LW, Holwell AK, Martin KL, Hewett KW, Gourdie RG. The rate and anisotropy of impulse propagation in the postnatal terminal crest are correlated with remodeling of Cx43 gap junction pattern. *Cardiovasc Res.* 2000;45:379-87.
3. Angst BD, Khan LU, Severs NJ, Whitely K, Rothery S, Thompson RP, Magee AI, Gourdie RG. Dissociated spatial patterning of gap junctions and cell adhesion junctions during postnatal differentiation of ventricular myocardium. *Circ Res.* 1997;80:88-94.
4. Price RL, Nakagawa M, Terracio L, Borg TK. Ultrastructural localization of laminin on in vivo embryonic, neonatal, and adult rat cardiac myocytes and in early rat embryos raised in whole-embryo culture. *J Histochem Cytochem.* 1992;40:1373-81.
5. Lukas J , Bartek J. Immunoprecipitation of proteins under non-denaturing conditions. In: Cellis JE, editor. *Cell Biology: A Laboratory Manual. 2nd ed. Vol.4.* New York: Academic Press, 1998. pp.489-94.
6. Gourdie RG, Green CR, Severs NJ. Gap junction distribution in adult mammalian myocardium revealed by an anti-peptide antibody and laser scanning confocal microscopy. *J Cell Sci.* 1991;99:41-55.
7. Nguyen-Tran VT, Kubalak SW, Minamisawa S, Fiset C, Minamisawa S, Fiset C, Wollert KC, Brown AB, Ruiz-Lozano P, Barrere-Lemaire S, Kondo R., Norman LW, Gourdie RG, Rahme MM, Feld GK, Clark RB, Giles WR, Chien KR. A novel genetic

pathway for sudden cardiac death via defects in the transition between ventricular and conduction system cell lineages. *Cell*. 2000;102(5):671-682.

Data Supplement Figure 1

